Chemistry & Biochemistry Faculty Publications   Chemistry & Biochemistry

2019

Atlas of Experimental and Theoretical High Temperature Methane Cross Sections from T = 295 to 1000K in the Near-Infrared

Andy Wong
Old Dominion University

Peter F. Bernath
Old Dominion University, pbernath@odu.edu

Michael Rey

Andrei V. Nikitin

Vladimir G. Tyuterev

Follow this and additional works at: https://digitalcommons.odu.edu/chemistry_fac_pubs

Part of the Astrophysics and Astronomy Commons, and the Physical Chemistry Commons

Atlas of Experimental and Theoretical High-temperature Methane Cross Sections from $T = 295$ to $1000\,\mathrm{K}$ in the Near-infrared

Andy Wong[1], Peter F. Bernath[1] , Michael Rey[2], Andrei V. Nikitin[3,4], and Vladimir G. Tyuterev[2,4]
[1] Department of Chemistry and Biochemistry, Old Dominion University, Norfolk, VA 23529, USA; pbernath@odu.edu
[2] Groupe de Spectrométrie Moléculaire et Atmosphérique, UMR CNRS 7331, BP 1039, F-51687, Reims Cedex 2, France
[3] Laboratory of Theoretical Spectroscopy, Institute of Atmospheric Optics, SB RAS, 634055 Tomsk, Russia
[4] QUAMER laboratory, Tomsk State University, 36 Lenin Avenue, 634050 Tomsk, Russia
Received 2018 August 7; revised 2018 October 21; accepted 2018 October 22; published 2019 January 4

Abstract

Spectra of hot methane were recorded using a tube furnace and a high-resolution Fourier transform spectrometer. We obtained experimental absorption spectra in the 1.85–1.11 μm near-infrared region at eight temperatures ranging from 295 K up to 1000 K. We have converted these into an atlas of absorption cross sections at each temperature for the methane tetradecad, icosad and triacontad polyads, excluding some spectral intervals either strongly contaminated by water or due to baseline fringes. On the theoretical side, the spectra were simulated from the ab initio-based Reims-Tomsk TheoReTS line list for the same experimental conditions. This line list has been constructed by global variational calculations from potential energy and dipole moment surfaces followed by empirical line position corrections deduced from previously published analyses. The comparisons showed very good overall agreement between observations and theory at high spectral resolution for the tetradecad and icosad and at medium or low resolution above this range. A full set of the theoretical absorption cross sections is also included. Detailed temperature dependence of the methane absorption enables the efficient method of remotely probing the temperature of distant astronomical objects based on a comparison of relative signals in carefully selected spectral intervals. This first combined experimental and theoretical easy-to-use cross-section library in the near-infrared should be of major interest for the interpretation of current and future astronomical observations up to a resolving power of 100,000–300,000 in the range 6400–7600 cm^{-1} and a resolving power of 5000–10,000 in the higher wavenumber range up to 9000 cm^{-1}.

*Key words:* astronomical databases: miscellaneous – infrared: general – molecular data

Supporting material: tar.gz file

1. Introduction

Considering the cosmic abundance of carbon and hydrogen, and the thermodynamic stability of methane at low temperatures, it is no surprise that methane is found in numerous astronomical sources. In substellar objects, methane appears when the temperature drops below about 1500 K (Bailey 2014). The spectrum of hot methane in the near-infrared is the defining feature of T-type brown dwarfs (Oppenheimer et al. 1995; Nakajima et al. 2001; Kirkpatrick 2005; Legget et al. 2007). As the temperature drops further, methane persists in Y dwarfs (Cushing et al. 2011), and is a very prominent feature in the spectra of the giant planets and Titan (Mueller-Wodarg et al. 2008; Hirtzig et al. 2013; Bézard 2014; Rey et al. 2018). Methane is seen in emission from comets, where it has a rotational temperature of about 50 K (Mumma et al. 1996; Dello Russo et al. 2005). It has been detected by transit spectroscopy of the atmospheres of hot Jupiter exoplanets such as HD 189733b at temperatures of about 1100 K (Swain et al. 2008, 2009, 2010; Moses et al. 2011; Hu & Seager 2014). The launch of the *James Webb Space Telescope* (*JWST*, see jwst.stsci.edu) in 2021 will allow observations of exoplanet atmospheres with an unprecedented signal-to-noise ratio, spectral coverage, and spatial resolution (Greene et al. 2016; Baudino et al. 2017; Mollière et al. 2017). It has been recently shown that the development of cross-correlation methods provides much more comprehensive information on exoplanetary atmospheres (Kempton et al. 2014; Snellen et al. 2014) provided accurate high-resolution template spectra are available. Due to these trends in astronomical observations, there is an increasing need for reliable high-resolution laboratory data for methane over a wide spectral range and for high temperatures as reviewed in Tinetti et al. (2013), Bernath (2014), Fortney et al. (2016), and Tennyson & Yurchenko (2017). The current state of the spectroscopy of methane has recently been summarized in the paper describing the HITRAN 2016 database (Gordon et al. 2017).

Because of high molecular symmetry, 9 vibrational degrees of nuclear motion are grouped in 4 vibrational modes (ν_1, 2917 cm^{-1}; ν_2, 1534 cm^{-1}; ν_3, 3019 cm^{-1}; ν_4, 1306 cm^{-1}). Only the ν_3 and ν_4 fundamental modes would be allowed for uncoupled modes. In reality, various interactions organize the vibration–rotation energy levels into "polyads" that become increasingly perturbed as the energy and density of states increase. For example, the 7 μm region containing the coupled ν_2 and ν_4 bands is called the dyad. The 3.3 μm region is called the pentad because five modes interact (ν_1, ν_3, $2\nu_2$, $2\nu_4$, and $\nu_2+\nu_4$). Experimental high-temperature methane spectra in these regions have been reported in Nassar & Bernath (2003), Thiévin et al. (2008), Hargreaves et al. (2012, 2015), and Amyay et al. (2016, 2018, and references therein). In this paper, we have recorded spectra of hot methane in the near-infrared region (5200–9200 cm^{-1}, $1.92 - 1.08$ μm) that includes the tetradecad (6000 cm^{-1}, 1.6 μm), icosad (7500 cm^{-1}, 1.3 μm), and triacontad (8600 cm^{-1}, 1.1 μm) polyads. Previous measurements in this range have been recorded with cold or room-temperature samples; e.g., for the tetradecad (Nikitin et al. 2015, 2017a), icosad (Campargue et al. 2012; Rey et al. 2016b) and triacontad (Brown 2005; Béguier et al. 2015) except for the recent paper (Ghysels et al. 2018), reporting laser absorption experiments at $T = 1000\,\mathrm{K}$ in a limited interval near 1.7 μm, and the Fourier transform emission spectrum reported by Nassar & Bernath (2003). The
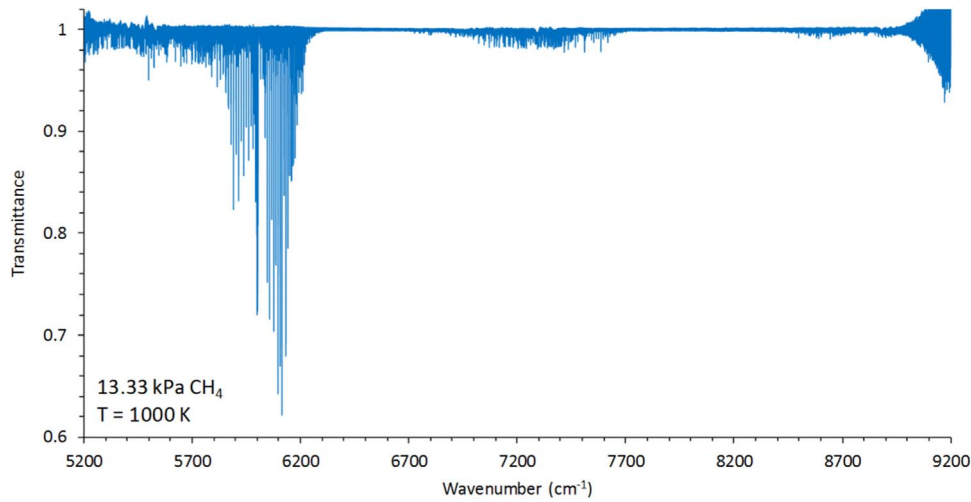
Figure 1. Overview spectrum of methane at 1000 K. The polyads can be seen near 5800 cm^{-1} (tetradecad), 7300 cm^{-1} (icosad), and 8800 cm^{-1} (triacontad).

most recent theoretical predictions in the near-infrared for hot methane are by Rey et al. (2017) and Yurchenko et al. (2017).

These two papers follow the suggestion of Hargreaves et al. (2015) to represent hot methane line lists with a set of strong and medium intensity lines, and to use a "quasi-continuum" (Rey et al. 2014, 2016a; Hargreaves et al. 2015) to account for the non-negligible opacity due to billions of weaker lines.

Various issues concerning the accuracy and consistency of theoretical models are debated in the literature (Rey et al. 2016a, 2017; Ghysels et al. 2018). It is also well known that obtaining billions of line parameters from laboratory observations alone is not feasible and purely empirical lists could thus suffer from completeness issues. Systematic inter-comparisons and validations of these two complementary sources of spectral information are necessary to provide reliable reference data for astrophysical applications and to evaluate their accuracy. In this work we provide the first atlas of methane absorption cross sections based both on laboratory measurements and ab initio theory. An extensive collection of easy-to-use files in a wide near-infrared region 6400–8900 cm^{-1} for eight temperatures ranging from 298 K up to 1000 K for astrophysical applications is included as electronic supplementary materials; these are also available at http://theorets.univ-reims.fr/files/supplementary/ApJ/ and http://cdsarc.u-strasbg.fr/viz-bin/qcat?J/ApJS.

2. Experimental

Spectra of hot methane (up to 1000 K) were recorded at Old Dominion University using a tube furnace, a quartz cell (optical path length of 50 cm), and a Bruker IFS 120/125HR (120 bench upgraded with 125 electronics) Fourier transform spectrometer. The spectrometer was equipped with a CaF$_2$ beamsplitter, a liquid N$_2$-cooled InSb detector, an optical filter, and an external halogen lamp to produce radiation covering a spectral range between 5200 and 9200 cm^{-1} (1.92 − 1.08 μm) (see Figure 1). A detailed description of the experimental setup can be found in Hargreaves et al. (2015). Experiments were performed at ambient temperature (295 K) without the use of the furnace and at elevated temperatures between 400 and 1000 at 100 K intervals. For these elevated temperatures, the furnace was set to the desired temperature and then left to stand for at least three hours to allow for thermal equilibration. Methane gas at

13.33 kPa (100 Torr) for each temperature was then introduced into the cell and monitored using a Baratron pressure gauge. For each temperature, 600 interferograms in total were recorded for both the sample and corresponding background at a resolution of 0.02 cm^{-1}. These were then averaged together and treated with a Norton-Beer weak apodization function and a zero-fill factor of two during the Fourier transformation. Final working spectra were then produced by applying a post-zero-fill factor of eight and subtraction of water lines to generate the transmission spectrum.

3. Theoretical

On the theoretical side, accurate calculations of radiative properties for high-temperature conditions require rovibrational energy levels and corresponding wavefunctions in a very large energy range that also provides the partition function $Q(T)$ *via* direct summation (Nikitin et al. 2015; Gamache et al. 2017) and Einstein coefficients for dipole transitions that provide line and band intensities for each T. Until recently, most analyses of experimental high-resolution methane spectra were based on empirical effective models for separate polyads; e.g., in Champion et al. (1992), Wenger & Champion (1998), Brown et al. (2013), Nikitin et al. (2017a), Amyay et al. (2018, and references therein). The polyads of vibrational states of methane are traditionally denoted P_n, where a lowercase n-index corresponds to the maximum number of the overtone-bending quanta involved. P_0 stands for the ground vibrational state, P_1 stands for the dyad (ν_2/ν_4), etc. Every vibrational state possesses rotational levels that depend on the total angular momentum quantum number J forming very dense rovibrational patterns strongly coupled by Coriolis and anharmonic interactions. Infrared methane spectra are partitioned into ranges of strong absorption/emission separated by so called "transparency windows." With increasing temperature, the complexity of spectra augments very rapidly. For example, in the tetradecad range, in addition to the "cold bands" (CB) corresponding to $P_4 - P_0$ transitions, a very important part of absorption/emission is due to "hot bands" (HB) among excited polyads $P_5 - P_1$, $P_6 - P_2$, etc., (Rey et al. 2017). In the icosad range CBs of the type $P_5 - P_0$ are in competition with HBs $P_6 - P_1$, $P_7 - P_2$ and so on. Moreover, the polyads are no longer decoupled and "windows" between them are no longer

transparent because of high-J and HB transitions. Up to now there have been no published line-by-line analyses for methane HBs in the near-infrared. Extrapolations using empirical models for high polyads suffer from severe accuracy and completeness issues (Rey et al. 2016a, 2017; Ghysels et al. 2018).

Recently, a breakthrough in the accuracy of ab initio calculations and the possibility of a dramatic increase in the completeness of first-principles variational spectral predictions has permitted the prediction of line parameters independent of (and complementary to) laboratory measurements. Several research teams have contributed to this progress, and as stated in the data-needs review of Tennyson & Yurchenko (2017): there are three groups that are systematically producing extensive theoretical line lists of key astronomical molecules. These are the NASA Ames group (Huang et al. 2017), the ExoMol group (Yurchenko et al. 2014; Tennyson et al. 2016), and the Reims-Tomsk group running the TheoReTS project (Rey et al. 2016a, 2017). Methane spectroscopy is a much harder problem than that for diatomic or triatomic molecules because there are more degrees of freedom in the vibration–rotation problem, which is much more difficult to solve, and the perturbations among spectral bands are much more extensive.

For this study we use a new high-temperature theoretical line list for $^{12}CH_4$ constructed by the Reims and Tomsk laboratories (Rey et al. 2017) in three steps. As a first step, over 150 billion transitions were generated with a lower rovibrational energy cutoff of $33,000 \, cm^{-1}$ by first-principles quantum mechanical variational calculations using the molecular potential energy surface of Nikitin et al. (2011, 2016). The line intensities were calculated from the purely ab initio dipole moment surfaces of Nikitin et al. (2017b). As a second step, empirical corrections for 3.7 million of the strongest transitions involving about 100,000 energy levels extracted from analyses of experimental laboratory room-temperature spectra were used to improve their line positions. At the third step, the calculated data were split into two sub-sets. "Light lists" contain strong and medium transitions necessary for accurate description of sharp features in absorption/emission spectra. For a fast and efficient modeling of quasi-continuum cross sections (Hargreaves et al. 2015; Rey et al. 2017), billions of weak lines are compressed in "superline"-libraries (Rey et al. 2016a).

4. Atlas of Experimental and Theoretical Absorption Cross Sections: Temperature Dependence

Raw experimental records cover the near-infrared range from 5200 to $9000 \, cm^{-1}$. We have converted these into observed absorption cross sections at selected temperatures for the methane tetradecad, icosad, and triacontad ranges. Because the aim of this publication is to provide reference data for astrophysical applications, we have excluded those spectral or temperature intervals that were strongly contaminated by water impurity lines or by remaining baseline fringes. The summary for experimental cross sections provided in the electronic supplementary materials is given in Table 1.

A full set of the theoretical absorption cross sections is also included in the atlas as given in Table 2. The theoretical simulations were done for the same conditions as the experimental records, but using Gaussian line-shape functions.
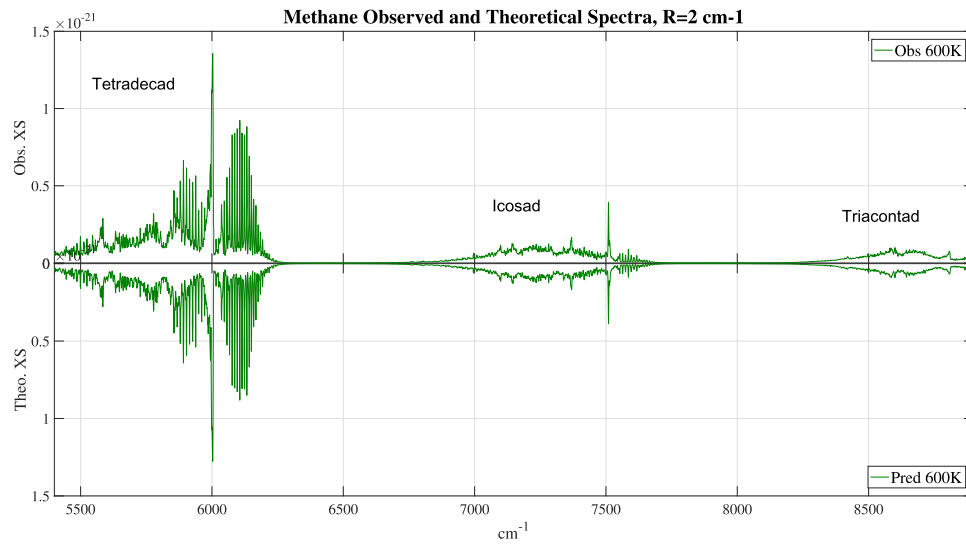
The aim in including theoretical cross sections was threefold: validate ab initio intensity predictions in the ranges of strong absorption, detect spectral intervals where observations

Table 1
Summary for Experimental Methane Absorption Cross Sections in $cm^2/molecule$ Provided in the Electronic Supplementary Materials

Obs.	Wavenumbers , cm^{-1}		
Temperature (K)	Tetradecad	Icosad	Triacontad
295	5495–6300	7415–7700	8250–8900
400	5550–6300	7415–7700	8200–8900
500	5740–6300	7430–7700	…
600	5400–6300	6600–7700	8200–8900
700	5583–6300	…	…
800	5955–6250	7500–7620	…
900	5938–6300	…	…
1000	5555–6300	7440–7700	8200–8900

were impacted by impurities or baseline issues, and extend spectral information beyond laboratory experimental data. In particular, in the 1.53 μm window (6300–6600 cm^{-1}) between the tetradecad and icosad and in the 1.25 μm window (7700–8200 cm^{-1}) between the icosad and triacontad, the signal-to-noise ratio of experimental records was not satisfactory. For a physically consistent determination of the baseline in the window regions, we have matched this to the ab initio absorbance simulated at very low resolution $\sim$100 cm^{-1} at far edges of the polyads in a way that the baseline would tend to nearly zero in the transparency windows. This was achieved by applying linear slope corrections, the aim being to constrain the baseline variation within the estimated signal-to-noise ratio (see Section 6). This did not affect experimental spectral features for medium and strong absorption (in the "hearts" of polyads), but it did help to avoid some artifacts, such as, for example, erratic negative absorbance. For the intervals summarized in Table 1 we were also able to remove some regular cosine-type fringes ("channeling") that are common in Fourier transform spectra. In the transparency windows, the experimental signal-to-noise ratio did not allow us to clearly distinguish between very weak methane absorption and remaining features due to baseline problems and impurities (mainly water vapor). For these reasons we do not provide experimental cross sections in the corresponding intervals between the tetradecad and the icosad, and between the icosad and the triacontad as specified in Table 1.

At medium and low spectral resolution, some overall absorption patterns and the contribution of the quasi-continuum, as well as the temperature dependence, are more clearly visible. For this reason, we include in the supplementary materials the reference cross sections at three resolutions. The first one has $R = 0.02 \, cm^{-1}$ (essentially determined by Doppler broadening at high-temperature) as experimentally recorded; the theoretical atlas uses a Gaussian line-shape function with a width of $0.02 \, cm^{-1}$. At medium ($R = 0.2 \, cm^{-1}$) and low ($R = 2 \, cm^{-1}$) resolution both experimental and theoretical cross sections were obtained in two steps: first the high-resolution transmittance files have been convoluted with the corresponding Gaussian "instrument functions," then they are converted to absorption cross sections. The data are provided in three tables in the electronic supplementary materials (Table S1 for experimental and Tables S2a and S2b for theoretical data; see also http://theorets.univ-reims.fr/files/supplementary/ApJ/ and http://cdsarc.u-strasbg.fr/viz-bin/qcat?J/ApJS.). The format and the volume of the point-by-point data file is given in Table 3.

Figure 2. Overview of methane observed and theoretical spectra at $T = 600$ K for the entire range of present experimental records, 5400–8900 cm^{-1}: absorption cross section (XS in cm^2/molecule) simulation with low resolution $R = 2$ cm^{-1}. Details for the three major absorbing intervals, 5400–6300 cm^{-1} ("tetradecad" range), 6400–7700 cm^{-1} ("icosad" range), and 8200–8900 cm^{-1} ("triacontad" range), are given in the next sections.

Table 2
Summary for Theoretical Methane Absorption Cross Sections in cm^2/molecule Provided in the Electronic Supplementary Materials

Theoretical Data in Supplementary Materials				
Eight temperatures	Full wavenumber range (cm^{-1})	N strong and medium lines included	QC including N super-lines	XS simulations for resolutions, R (cm^{-1})
From 295 to 1000 K (steps of 100 K)	5400−9000	$N = 11.8$ million	$N = 1.03$ billion	$R = 0.02$; $R = 0.2$; $R = 2$

Table 3
Format of Supplementary Point-by-point Cross-section Files

Columns	R = spectral resolution	T = temperature	Wn = wavenumber	XS = absorption cross section
units	cm^{-1}	K	cm^{-1}	cm^2/molec
Table S1		Experimental methane absorption XS − ASCII file size = 29 Mb (zipped), 158 Mb (unzipped)		
	$R = 0.02$, $R = 0.2$, $R = 2$	See Table 1	Average step = 0.007533 cm^{-1}	Total number of points = 4 047 349
Table S2a		Theoretical methane absorption XS − ASCII file size = 87 Mb (zipped), 480 Mb (unzipped)		
	$R = 0.02$	295–900 K (step of 100 K)	step = 0.002 cm^{-1}	Total number of points = 12 599 979
Table S2b		Theoretical methane absorption XS − ASCII file size = 87 Mb (zipped), 508 Mb (unzipped)		
	$R = 0.02$ $R = 0.2$, $R = 2$	1000 K 295−1000 K (step of 100 K)	step = 0.002 cm^{-1} step = 0.005 cm^{-1}	Total number of points = 13 319 983

5. Overview Comparison of Observed and Theoretical Absorption Cross Sections under High, Medium, and Low Resolutions

As mentioned above, it was difficult to avoid contamination of the observed spectra by strong water lines at the lower end of the tetradecad (below 5500 cm^{-1}) and in the lower part of the icosad (below 7400 cm^{-1}) for most temperatures, except for 600 K. Figure 2 gives the comparison between experimental and ab initio cross sections for the entire wavenumber range of this atlas 6400–8900 cm^{-1} at 600 K. The resolution was degraded to

2 cm^{-1} to have a global overview of major features in three of the absorption intervals: tetradecad, icosade and triacontad. Separate zoomed-in views for each range at high, medium, and low resolution, as well as the temperature dependence, are considered in the next sections.

5.1. Tetradecad Range (5400–6300 cm^{-1})

The tetradecad is the strongest absorption range of the present atlas, and the experimental data are much more complete here, permitting a very detailed validation of the

theory. Six R-branch lines from 6036 to 6086 cm^{-1} in the room-temperature and 400 K spectra were slightly saturated, and corrections were made using the corresponding HITRAN 2016 lines. We do not claim that our atlas provides experimental information for these few absorption features at 300 and 400 K. For higher temperatures and for other spectral ranges, the lines were not saturated. The overview comparison of the entire tetradecad range at four temperatures in Figure 3(a) clearly shows how the spectral interval is dominated by hot or cold bands. This is even more visible for the expanded scales in Figures 3(b)–5. Our atlas can be used to select particular spectral ranges that show strong absorption or a strong temperature dependence of the absorption for future astronomical observations.

For example, Figure 3(b) in the 5900–6250 cm^{-1} interval at $R = 2$ cm^{-1} is very useful for practical astrophysical applications. This shows that the detailed temperature dependence from $T = 300$ to 1000 K with 100 K steps is fully consistent between observations and theory. One can clearly conclude that the Q-branch of the $2\nu_3$ cold fundamental band at 6000 cm^{-1} remains dominant at 300 K, whereas the absorption just below at 5940–5960 is dominant at high $T = 900$–1000 K. Strong absorption features between 6050 and 6100 cm^{-1} are the most pronounced for 400–500 K, in the next range 6100–6130 cm^{-1} for 500–600 K, then in 6050–6100 cm^{-1} for 700–900 K and above this range for 1000 K.

The full T-dependence in the central part of the tetradecad at medium resolution ($R = 0.2$ cm^{-1}) is given in Figure 4. This shows the intervals in which absorption increases with temperature, whereas it could be the opposite for neighboring strong cold band multiplets. Finally, Figures 5(a)–(d)) compare experimental and theoretical tetradecad spectra at the original resolution of the observations ($R = 0.02$ cm^{-1}). Figures 5((a)–(c)) show a global view of the tetradecad, as well as expanded views of its lower and central sections. This was plotted at only two temperatures to avoid confusing figures. The full high-resolution T-dependence with eight temperatures at the tetradecad center near 6000 cm^{-1} is shown in Figure 5(d).

5.2. Icosad Range (6600–7700 cm^{-1})

Experimental reference cross sections for the full icosad range are only provided at 600 K, because of baseline issues and strong water contamination in this interval for other temperatures. The full overview icosad comparison is given in Figure 2. For the upper part of the icosad the experimental cross sections are provided for six temperatures (see Table 1). However, the theoretical cross sections cover the entire range. Low-, medium-, and high-resolution comparisons given in Figure 6 clearly show that theoretical cross sections are reliable for the most important features and could safely also be used in the intervals where the reference experimental impurity-free cross sections are not provided.

### 5.3. Triacontad Range (8200–8900 cm^{-1})

The highest polyad range of the atlas corresponds to much weaker absorption than in the tetradecad and in the icosad (see Figure 2), but still important for long optical atmospheric paths and thus of significant interest for astrophysical applications. No line-by-line analyses of laboratory experiments spectra are available in this range.

Theory predicts 280 vibrational cold bands (Tyuterev et al. 2013) of $P_6 - P_0$ type and many thousand hot bands $P_7 - P_1$, $P_8 - P_2$, etc., (Rey et al. 2017) falling together in the triacontad range. The superposition of their rovibrational transitions form very dense complex patterns. The absence of experimental assignments, even for cold bands, does not allow empirical line position corrections. Because of the lower signal-to-noise ratio in experiments and larger uncertainties in high-energy predictions, it is recommended that the atlas data be used for medium- and low-resolution applications. Figure 7 shows that at resolutions of $R = 0.2$ cm^{-1} and $R = 2$ cm^{-1} in the triacontad range, there is still a good qualitative consistency between ab initio theory and observation for the frequency and temperature dependence of the methane opacity.

6. Discussion and Conclusions

We provide here the first extensive atlas of methane absorption cross sections in a wide near-infrared region 1.92–1.08 μm for eight temperatures ranging from 295 K up to 1000 K for astrophysical applications. The experimental part of the atlas is based on laboratory Fourier transform spectra recorded with a resolution of 0.02 cm^{-1}. A full set of theoretical ab initio absorption cross sections is also included in the atlas. The comparisons show very good overall agreement between observations and theory at high spectral resolution for the tetradecad and icosad and at medium or low resolution for the triacontad. But the two do not coincide exactly for smaller features. This can be seen at the weak edges of polyads or in the intervals that are not dominated by strong lines. The deviations in line positions or in band centers naturally increase toward higher wavenumbers, as seen in the triacontad range (Figure 7), or at the upper edge of the icosad near 7485, 7520 cm^{-1} or above 7560 cm^{-1} (Figures 6(b); (c)). This is because the calculation error for high-J transitions increases, and also because most rovibrational energy levels corresponding to hot band transitions beyond the tetradecad are not experimentally known. Even if the intensity predictions are globally correct, the line position errors for small lines could produce some artificial overlapping enhancing or decrease the strength of the apparent features. In order to use our observed data to extend empirical optimization of the line positions in the calculated lists, a detailed line-by-line analysis must be performed. This requires a huge effort over many years, as even room-temperature and cold spectra beyond 7600 cm^{-1} are still not assigned. In the supplementary material, all data are provided in simple point-by-point text format that enables the user to easily make plots for further comparisons.

The experimental and theoretical data are complementary because theoretical spectra that cover uniformly all temperatures and wavenumber ranges help to fill gaps in the observations, in particular giving the temperature dependence in windows that are no longer transparent at high temperatures. Both experimental and theoretical atlas data can be safely used in spectral intervals where the discrepancy between cross sections is smaller than the uncertainty of astronomical observations, i.e., for most strong absorption/emission features. If this is not the case, the experimental data are preferred for small and medium features, which are clearly above the noise level. For systems in thermodynamic equilibrium, emission spectra can be readily computed (Bernath 2016) from absorption cross sections in the present atlas. The strongest absorption/emission features have a tendency to decrease with

(a)

(b)
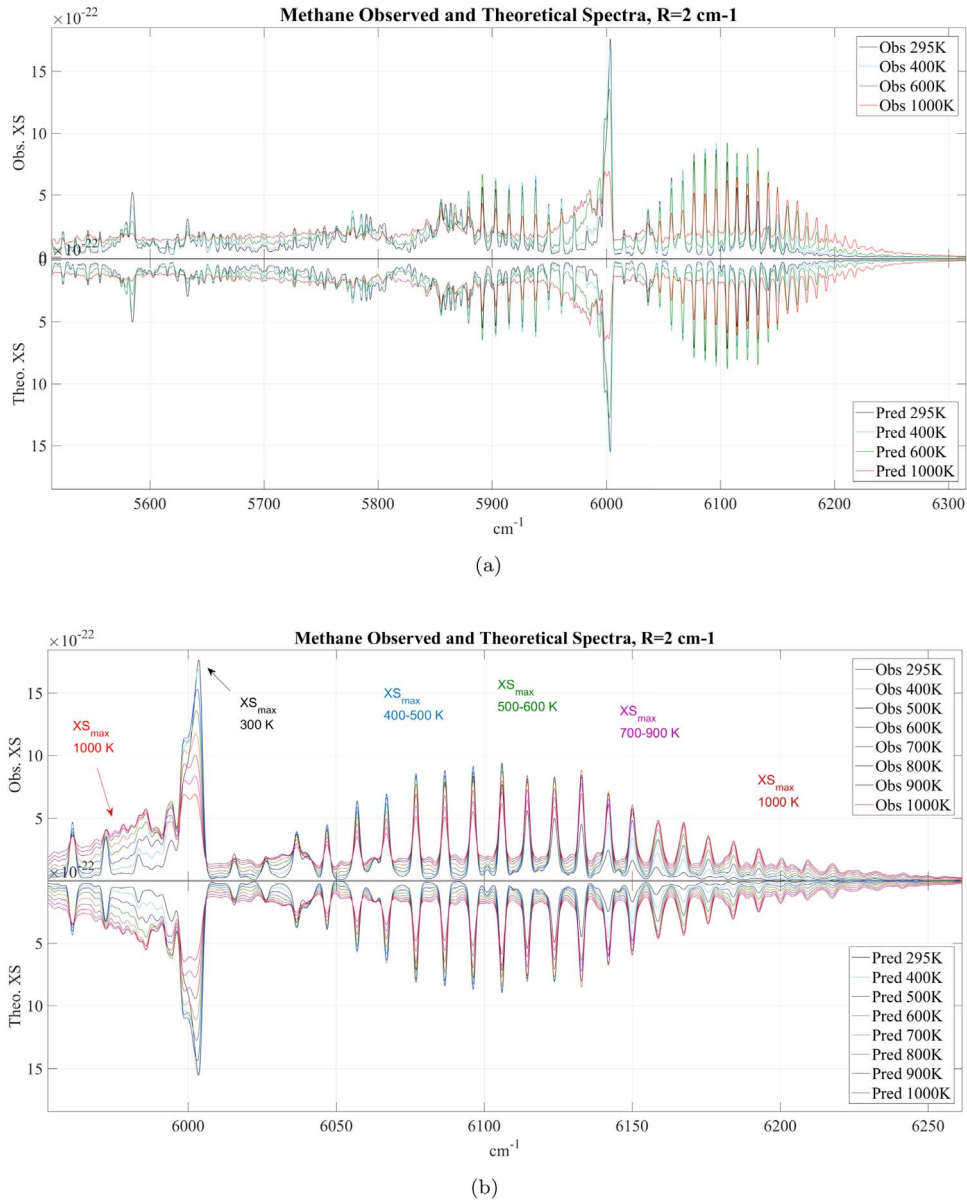
Figure 3. Panel (a): overview of absorption cross sections (cm^2/molecule) of methane in the tetradecad range 5400–6300 cm^{-1} at four temperatures, $T = 295, 400,$ 600, and 1000 K: low resolution ($R = 2$ cm^{-1}) simulations of observations (up) and theory (down). Panel (b): absorption cross sections (cm^2/molecule) of methane in the strong absorbing range around 6000 cm^{-1} at eight temperatures, $T = 295, 300, 400, 500, 600, 700, 800, 900,$ and 1000 K: low resolution ($R = 2$ cm^{-1}) simulations of observations (up) and theory (down). Dominant absorption features are clearly temperature-dependent, and their relative strengths could be used for fast temperature retrievals.

the temperature because of the partition function $Q(T)$, but the quasi-continuum is increasing, and hot bands and high-J lines emerge in various intervals. The atlas gives a consistent picture between observation and theory for these effects. This provides an efficient method of remotely probing the temperature of distant astronomical objects by comparing the relative intensity in carefully selected spectral intervals. For example, by comparing the ratios for astronomical observations with the ratios of the atlas cross sections in successive spectral intervals specified in Figure 3(b), one could determine an effective temperature. To implement this procedure in a robust way one needs reliable temperature-dependent spectroscopic data that are consistent between observations (impurity-free) and calculations (validated by experiment). The aim of this atlas is to provide a set of such easy to use cross sections. The good agreement with experiment suggests that the complete

line lists of the TheoReTS information system (Rey et al. 2016a, 2017) could provide correct data for temperatures above 1000 K.

The full accessibility of both the observed and calculated cross sections provided in the supplementary materials will allow more detailed comparisons and validation with other experimental and theoretical sources of methane data. It has already been shown in many previous studies that HITRAN, GEISA, or similar databases designed for room-temperature or colder applications serve as good starting points for some relatively isolated lines, but the huge number of missing hot bands and high-J transitions may lead to erroneous conclusions for hot samples. Bailey & Kedziora-Chudczer (2012) showed that these missing high-temperature transitions result in substantial missing opacity in brown dwarf models if such incomplete line lists are used.
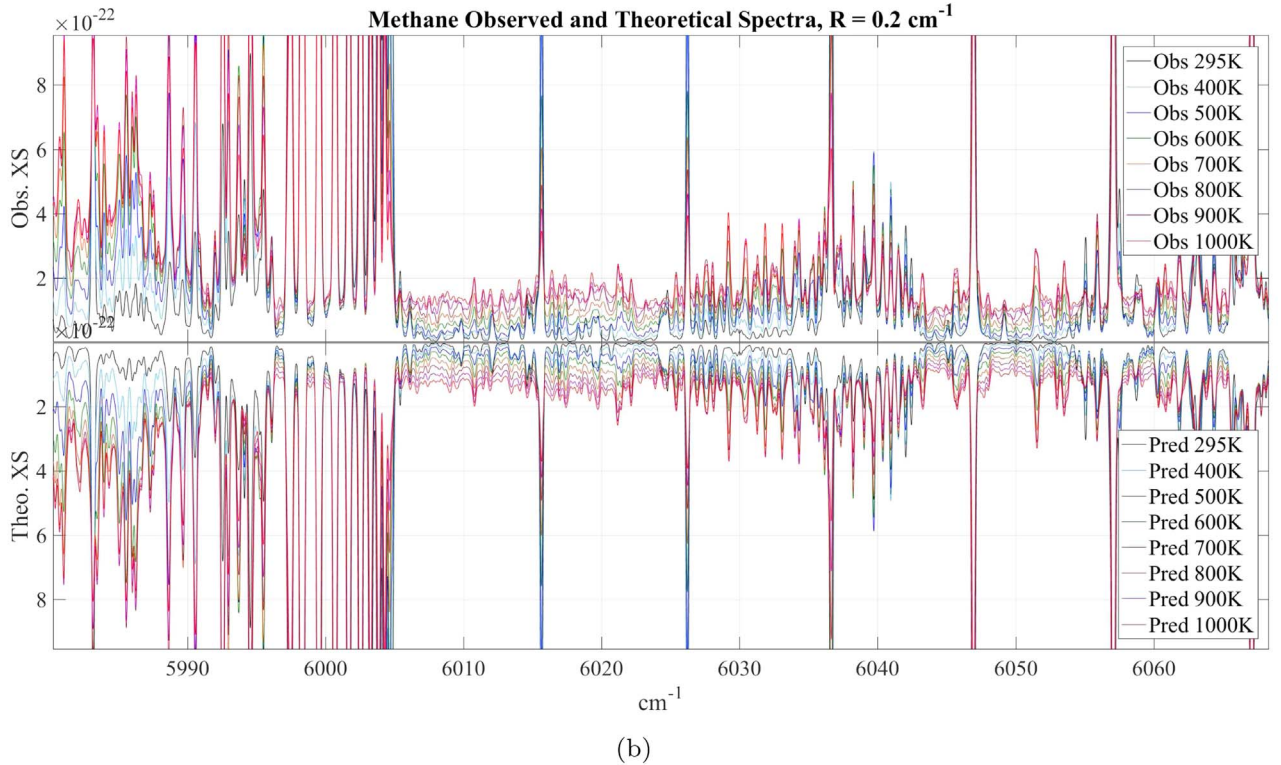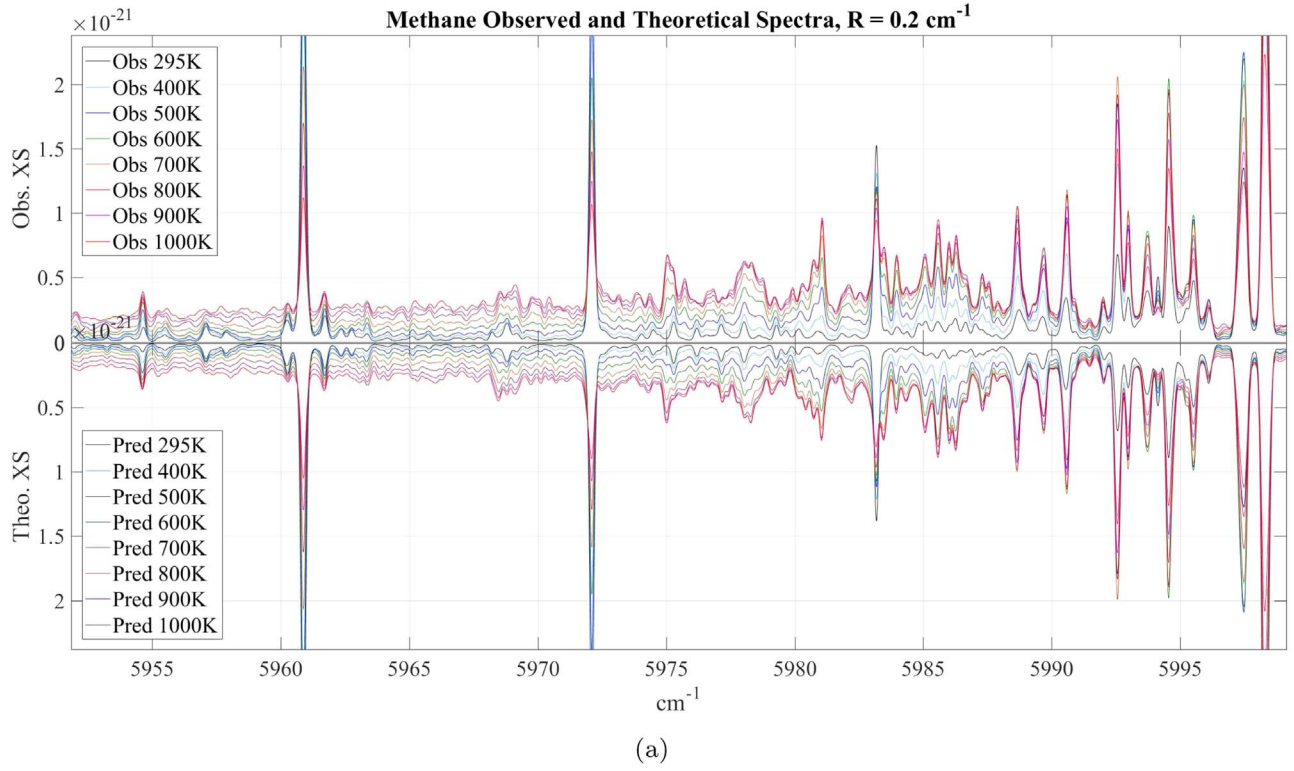
Figure 4. Panel (a): *T*-dependence of absorption cross sections (cm^2/molecule) of methane in the central part of the tetradecad at eight temperatures 295, 300, 400, 500, 600, 700, 800, 900, and 1000 K: medium resolution (*R* = 0.2 cm^{-1}) simulations of observations (up) and theory (down). Panel (b): *T*-dependence of methane absorbance in the strong tetradecad range at eight temperatures 295, 300, 400, 500, 600, 700, 800, 900, and 1000 K: expanded cross-section simulations under medium resolution (*R* = 0.2 cm^{-1}) of observations (up) and theory (down).

Much effort has recently been devoted to the calculation of high-temperature methane data such as the UCL ExoMol list (Yurchenko et al. 2014, 2017) using ab initio intensities, and the Dijon MeCaSDa list accessible via the VAMDC web portal

(Ba et al. 2013; Dubernet et al. 2016) based on extrapolation of experimental analyses (Amyay et al. 2018), and the TheoReTS list using RNT-2017 ab initio intensities. Quite significant discrepancies exist among these calculations, as discussed by
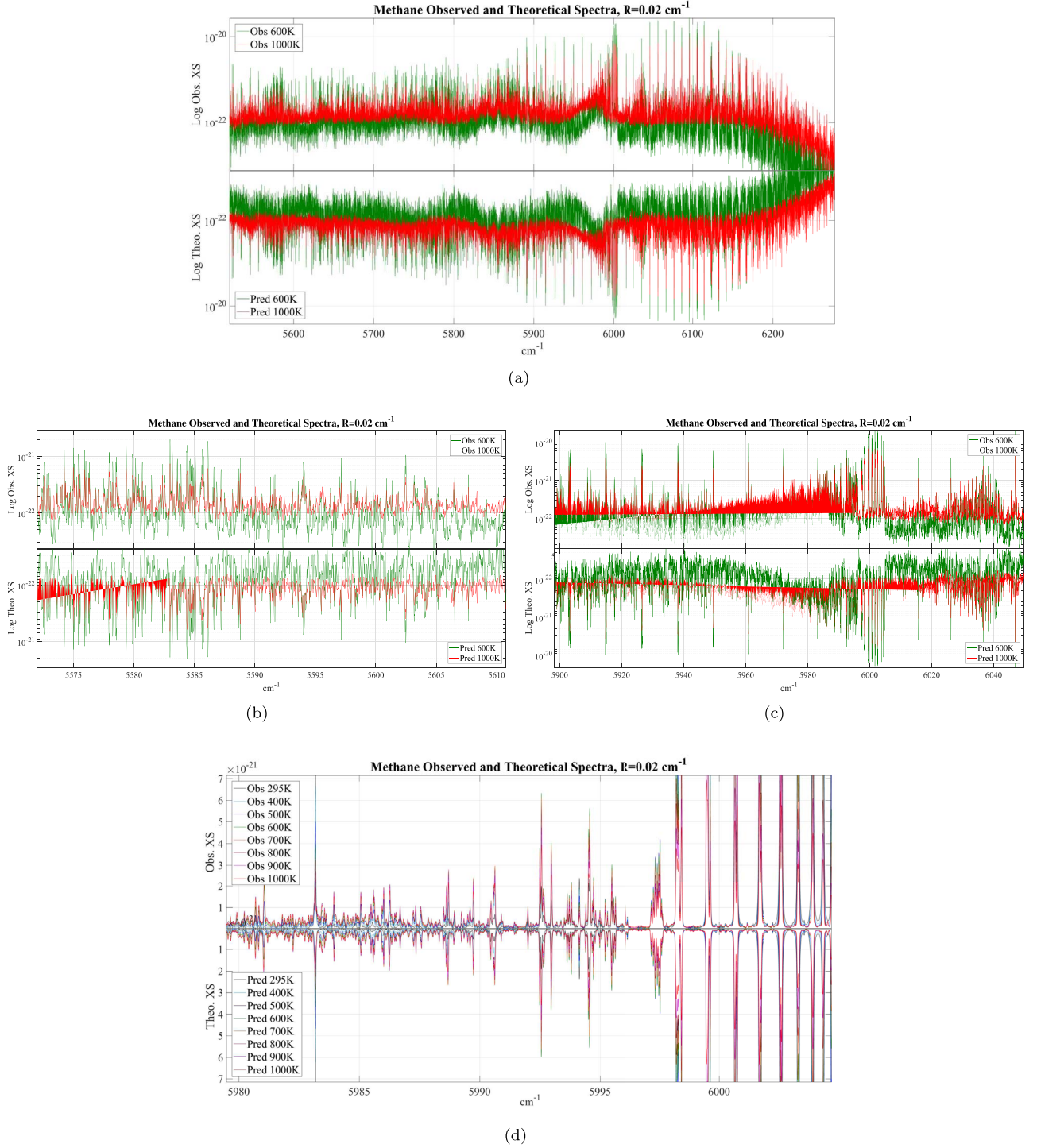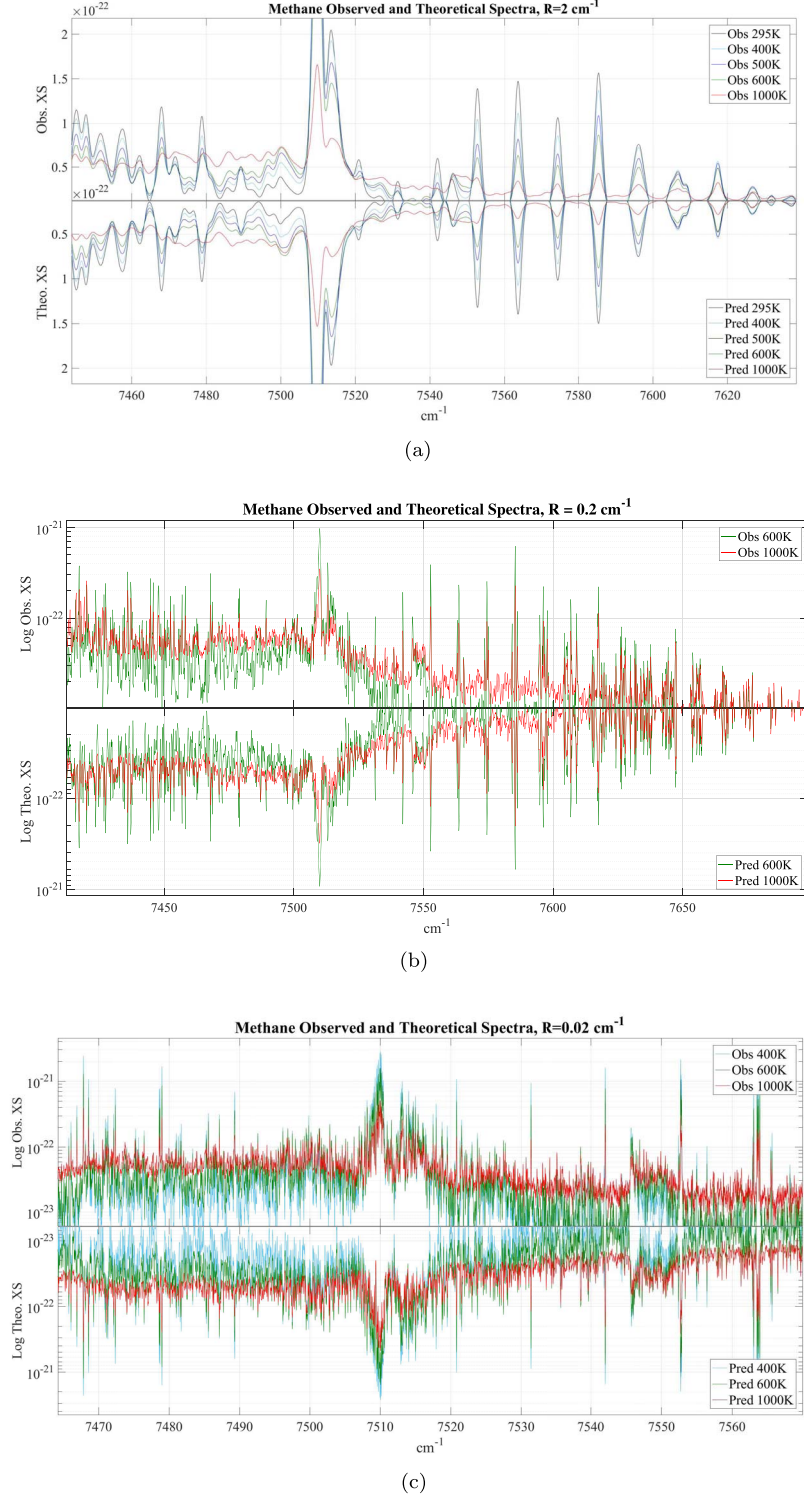
Figure 5. Panel (a): high-resolution ($R = 0.02\ \mathrm{cm}^{-1}$) log-scale comparison between observations (up) and the theory (down) for the methane absorption cross sections (cm^2/molecule) in entire tetradecad range at two temperatures $T = 600$ K (green), and $T = 1000$ K (red). Panel (b): high-resolution ($R = 0.02\ \mathrm{cm}^{-1}$) comparison between observations (up) and the theory (down) for the methane absorption cross sections in the lower part of the tetradecad at two temperatures $T = 600$ K (green), and $T = 1000$ K (red). Panel (c): high-resolution ($R = 0.02\ \mathrm{cm}^{-1}$) comparison between observations (up) and the theory (down) for the methane absorption cross sections in the middle part of the tetradecad at two temperatures $T = 600$ K (green), and $T = 1000$ K (red). Panel (d): T-dependence of methane absorbance in the middle part of tetradecad at 8 temperatures, 295, 300, 400, 500, 600, 700, 800, 900, and 1000 K: comparison of observed (up) and theoretical (down) absorption cross sections under high resolution ($R = 0.02\ \mathrm{cm}^{-1}$).

Rey et al. (2014, 2017, 2018), and Nikitin et al. (2018), particularly at high and medium resolutions. Hargreaves et al. (2015) have compared observations of hot spectra in the 3 μm range with ab initio calculations available at that time.

Recently, Ghysels et al. (2018) reported a comparison of their observed 1000 K laser methane spectra in the upper part of the tetradecad with HITRAN2016 and with all available calculations, and also found that the TheoReTS list gave the

(a)

(b)

(c)

Figure 6. Panel (a): T-dependence of absorption cross sections (cm^2/molecule) of methane in the upper part of the icosad at five temperatures, 295, 400, 500, 600, and 1000 K: low-resolution ($R = 2$ cm^{-1}) simulations of observations (up) and theory (down). Panel (b): log-scale comparison of observed (up) and theoretical (down) methane absorption cross sections at the upper edge of the icosad for two temperatures $T = 600$ K (green) and 1000 K (red): medium-resolution ($R = 0.2$ cm^{-1}) simulations. Panel (c): high-resolution ($R = 0.02$ cm^{-1}) comparison between observations (up) and the theory (down) for the methane cross sections for the strongest absorption features of the icosad at three temperatures $T = 400$ K (blue), $T = 600$ K (green), and $T = 1000$ K (red).

most consistent results. A very good agreement between our experimental spectra with the TheoReTS predictions confirms that this conclusion remains valid over the larger wavenumber and temperature range of the present atlas.

An important point concerns the uncertainty and limitations of the atlas. Various extensive comparisons and simulations, including cold and room-temperature measurements and laboratory analyses, suggest that the "noise level" in the cross
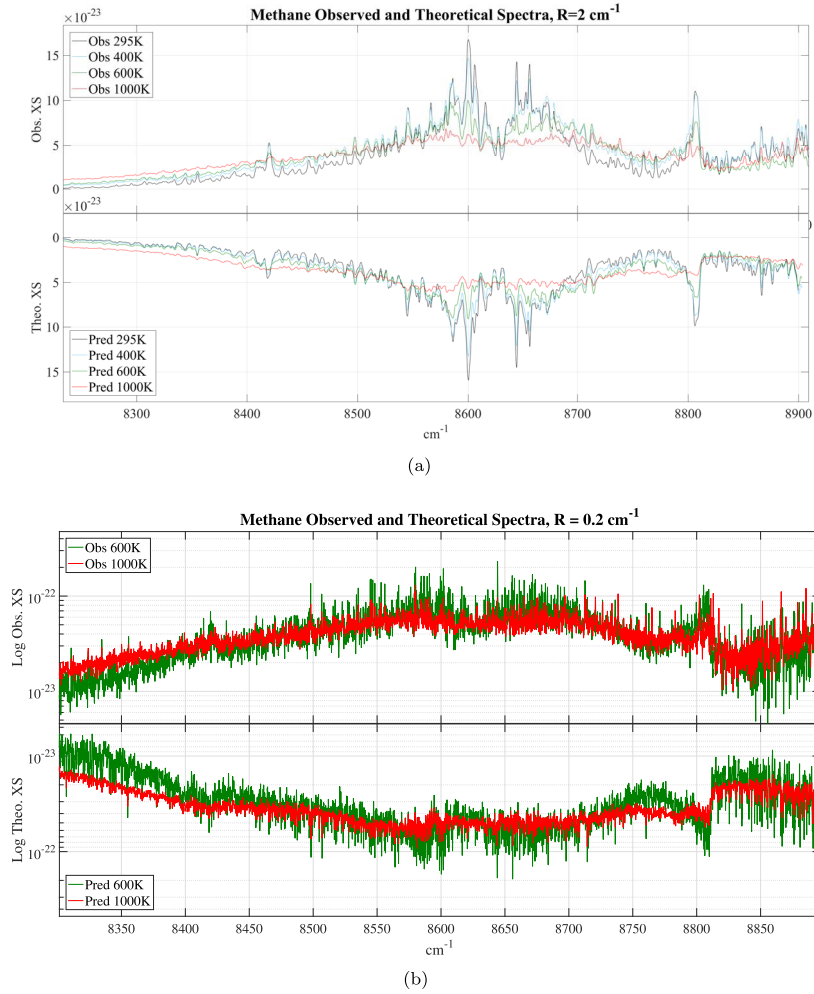
Figure 7. Panel (a): an overview of the T-dependence of methane absorption cross sections (cm^2/molecule) in the triacontad range at four temperatures 295, 400, 600, and 1000 K: low-resolution ($R = 2$ cm^{-1}) simulations of observations (up) and theory (down). Panel (b): log-scale comparison of observed (up) and theoretical (down) methane absorption X-sections at the triacontad range for two temperatures $T = 600$ K (green) and 1000 K (red): medium-resolution ($R = 0.2$ cm^{-1}) simulations.

sections is 10^{-23}–10^{-24} cm^2/molecule depending on the interval. This is linked to various issues related to impurities and baseline artifacts in the observations and to uncertainties in the calculations. We do not recommend using our cross sections below this noise level. This was one of the reasons to exclude some spectral intervals from the experimental data in the atlas (Table 1). On the theoretical side, the uncertainties are gradually increasing for high-J transitions and hot bands involving polyads P_6, P_7, $\cdots$ as is seen, for example, at the right edge of Figures 6(b) and 7. However, the signal-to-noise ratio of the atlas is certainly appropriate for astronomical observations. For high-resolution data, we estimate the signal-to-noise ratio to be 10^3 in the tetradecad, 10^2 in the icosad, and 10–20 for the triacontad. Our atlas data can be recommended for the interpretation of current or future astronomical observations up to a resolving power of 100,000–300,000 in the range 6400–7600 cm^{-1} and a resolving power of 5000–10,000 at higher wavenumbers up to 8900 cm^{-1}.

ORCID iDs

Peter F. Bernath ⬤ https://orcid.org/0000-0002-1255-396X

References

Amyay, B., Georges, R., Bienner, L., et al. 2018, JChPh, 148, 134306
Amyay, B., Louviot, M., Pirali, O., et al. 2016, JChPh, 144, 024312
Ba, Y. A., Wenger, C., Surleau, R., et al. 2013, JQSRT, 130, 62
Bailey, J. 2014, PASA, 31, e043
Bailey, J., & Kedziora-Chudczer, L. 2012, MNRAS, 419, 1913
Baudino, J.-L., Mollière, P., Venot, O., et al. 2017, ApJ, 850, 150
Béguier, S., Liu, A. W., & Campargue, A. 2015, JQSRT, 166, 6
Bernath, P. 2014, RSPTA, 372, 20130087
Bernath, P. 2016, Spectra of Atoms and Molecules (3rd ed.; Oxford: Oxford Univ. Press)
Bézard, B. 2014, Icar, 242, 64
Brown, L. 2005, JQSRT, 96, 251
Brown, L. R., Sung, K., Benner, D. C., et al. 2013, JQSRT, 130, 201
Campargue, A., Leshchishina, O., Wang, L., et al. 2012, JQSRT, 113, 1855
Champion, J. P., Loete, M., & Pierre, G. 1992, in Spherical Top Spectra, ed. K. N. Rao & A. Weber (San Diego: Academic)

Cushing, M. C., Kirkpatrick, J. D., Gelino, C. R., et al. 2011, ApJ, 743, 50
Dello Russo, N., Bonev, B. P., DiSanti, M. A., et al. 2005, ApJ, 621, 537
Dubernet, M. L., Antony, B. K., Ba, Y. A., et al. 2016, JPhB, 49, 074003
Fortney, J. J., Robinson, T. D., Domagal-Goldmal, S., et al. 2016, arXiv:1602.06305
Gamache, R. R., Roller, C., Lopes, E., et al. 2017, JQSRT, 203, 70
Ghysels, M., Vasilchenko, S. S., Mondelain, D., et al. 2018, JQSRT, 215, 59
Gordon, I. E., Rothman, L. S., Hill, C., et al. 2017, JQSRT, 203, 3
Greene, T. P., Line, M. R., Montero, C., et al. 2016, ApJ, 817, 17
Hargreaves, R. J., Beale, C. A., Michaux, L., Irfan, M., & Bernath, P. F. 2012, ApJ, 774, 89
Hargreaves, R. J., Bernath, P. F., Bailey, J., & Dulick, M. 2015, ApJ, 813, 12
Hirtzig, M., Bézard, B., Lellouch, E., et al. 2013, Icar, 226, 470
Hu, R., & Seager, S. 2014, ApJ, 784, 63
Huang, X., Schwenke, D. W., Freedman, R. S., et al. 2017, JQSRT, 203, 224
Kempton, E. M. R., Pern, R., & Heng, K. 2014, ApJ, 795, 24
Kirkpatrick, J. D. 2005, ARA&A, 43, 195
Legget, S. K., Marley, M. S., Freedman, R., et al. 2007, ApJ, 667, 537
Mollière, P., van Boekel, R., Bouwman, J., et al. 2017, A&A, 600, A10
Moses, J. I., Visscher, C., Fortney, J. J., et al. 2011, ApJ, 737, 15
Mueller-Wodarg, I. C. F., Strobel, D. F., Moses, J. I., et al. 2008, SSRv, 139, 191
Mumma, M. J., DiSanti, M. A., Dello Russo, N., et al. 1996, Sci, 272, 1310
Nakajima, T., Tsuji, T., & Yanagisawa, K. 2001, ApJ, 561, L119
Nassar, R., & Bernath, P. 2003, JQSRT, 82, 279
Nikitin, A. V., Chizhmakova, I. S., Rey, M., & Tyuterev, Vl. G. 2017a, JQSRT, 203, 341
Nikitin, A. V., Krishna, B. M., Rey, M., Tashkun, S. A., & Tyuterev, Vl. G. 2015, JQSRT, 167, 53
Nikitin, A. V., Lyulin, O. M., Mikhailenko, S. N., et al. 2015, JQSRT, 154, 63
Nikitin, A. V., Protasevich, A. E., Rey, M., & Tyuterev, Vl. G. 2018, JChPh, 149, 124305
Nikitin, A. V., Rey, M., & Tyuterev, Vl. G. 2011, CPL, 501, 179
Nikitin, A. V., Rey, M., & Tyuterev, Vl. G. 2016, JChPh, 145, 114309
Nikitin, A. V., Rey, M., & Tyuterev, Vl. G. 2017b, JQSRT, 200, 90
Oppenheimer, B. R., Kulkarni, S. R., Matthews, K., & Nakajima, T. 1995, Sci, 270, 1478
Rey, M., Nikitin, A. V., Babikov, Y. L., & Tyuterev, Vl. G. 2016a, JMoSp, 327, 138
Rey, M., Nikitin, A. V., Bézard, B., et al. 2018, Icar, 303, 114
Rey, M., Nikitin, A. V., Campargue, A., et al. 2016b, PCCP, 18, 176
Rey, M., Nikitin, A. V., & Tyuterev, Vl. G. 2017, ApJ, 847, 105
Rey, M., Nikitin, A. V., & Tyuterev, Vl. 2014, ApJ, 789, 2
Snellen, I. A. G., Brandl, B. R., de Kok, R. J., et al. 2014, Natur, 509, 63
Swain, M. R., Deroo, P., Griffith, C. A., Tinetti, G., et al. 2010, Natur, 463, 637
Swain, M. R., Vasisht, G., & Tinetti, G. 2008, Natur, 452, 329
Swain, M. S., Vasisht, G., Tinetti, G., et al. 2009, ApJ, 690, L114
Tennyson, J., & Yurchenko, S. N. 2017, MolAs, 8, 1
Tennyson, J., Yurchenko, S. N., Al-Refaie, A. F., et al. 2016, JMoSp, 327, 73
Thiévin, J., Georges, R., Carles, S., et al. 2008, JQSRT, 109, 2027
Tinetti, G., Coustenis, A., & Encrenaz, Th. 2013, A&ARv, 21, 63
Tyuterev, Vl. G., Tashkun, S., Rey, M., et al. 2013, JPCA, 117, 13779
Wenger, C., & Champion, J.-P. 1998, JQSRT, 59, 471
Yurchenko, S. N., Amundsen, D. S., Tennyson, J., & Waldmann, I. P. 2017, A&A, 605, A95
Yurchenko, S. N., Tennyson, J., Bailey, J., et al. 2014, PNAS, 111, 9379